Supporting information

Engineering the oxygen-evolution activity by changing the A-site rare-earth element in $RSr_3Fe_{1.5}Co_{1.5}O_{10-\delta}$ (R=La, Nd, Pr) Ruddlesden-Popper perovskites

Wenyun Zhu,[1] Jiani Chen,[1] Dongliang Liu,[1] Guangming Yang,[1] Wei Zhou,[1] Ran Ran,[1] Jie Yu,[2, 3, *] Zongping Shao [1,4,*]

1. *A State Key Laboratory of Materials-Oriented Chemical Engineering, College of Chemical Engineering, Nanjing Tech University, Nanjing, 210009, China*

2. *School of Energy and Power, Jiangsu University of Science and Technology, Zhenjiang 212100, P. R. China*

3. *Department of Building and Real Estate, Research Institute for Sustainable Urbanization (RISUD), Research Institute for Smart Energy (RISE), The Hong Kong Polytechnic University, Hung Hom, Kowloon, Hong Kong, 999077, P. R. China*

4. *WA School of Mines: Minerals, Energy and Chemical Engineering, Curtin University, Perth 6102, Australia.*

1. Experimental section

1.1. Material synthesis

The RP perovskite $LaSr_3Co_{1.5}Fe_{1.5}O_{10-\delta}$(LSFC), $NdSr_3Co_{1.5}Fe_{1.5}O_{10-\delta}$(NSFC), $PrSr_3Co_{1.5}Fe_{1.5}O_{10-\delta}$(PSFC) were obtained through a sol-gel method, with ethylenediaminetetraacetic acid (EDTA) and citric acid (CA) as complexing agent. With the preparation of LSCF as an example, stoichiometric amount of $La(NO_3)_3{\cdot}6H_2O$ (Aladdin Chemical Reagent Co., Ltd.), $Sr(NO_3)_2$ (Sinopharm Reagent Co., Ltd.), $Co(NO_3)_2{\cdot}6H_2O$ (Sinopharm Reagent Co., Ltd.) and $Fe(NO_3)_3{\cdot}9H_2O$ (Sinopharm Reagent Co., Ltd.) was weighed and stirred until the materials were completely dissolved in deionized water. Afterward, EDTA ($C_{10}H_{16}N_2O_8$, Sinopharm Reagent Co., Ltd.) and CA ($C_6H_8O_7{\cdot}H_2O$, Sinopharm Reagent Co., Ltd.) was dissolved into an NH_3 aqueous solution ($NH_3{\cdot}H_2O$, Sinopharm Reagent Co., Ltd.), wherein total metal ions, EDTA, CA were at a mole ratio of 1:1:2 and the ammonium hydroxide was used to adjust the PH to 6-7 to gain complexing agent solution, which was added into former solution. The solution was heat at 90℃ under stirring by a two-way magnetic heating stirrer (79-2, Changzhou Guohua Electric Co., Ltd.) till a pellucid gel took shape. The temperature of the gel was kept at 180℃ in an electric blast drying oven (101A-1E, Shanghai Yiheng Scientific Instrument Co., Ltd.) for 8h to derive a solid precursor. Eventually, crushed the precursors

and calcined at 1350℃ in the air for 12h in a muffle furnace (KF1700-I, Nanjing Boyuntong Scientific Instrument Co., Ltd.) to derive pure-phase powers.

1.2. Characterization

XRD patterns were collected using an X-ray diffractometer (Smart Lab, Germany Bruker) equipped with a Cu target (wavelength of k_α radiation is 1.5418Å). The scanning angle 2θ ranges from 10˚ to 90˚ with a scanning speed of 20˚ min^{-1}. XPS curves were obtained by X-ray Photoelectron Spectrometer (PHI5000, PHI Instruments, Inc.). Nitrogen adsorption-desorption curve was obtained at the boiling point (77K) of liquid nitrogen with BELSORP-mini, (Bel Japan, Inc.) source. The specific surface area was obtained based on the Branauer Emmett Teller (BET) method. Inductively coupled plasma-mass spectroscopy (ICP-MS) results were conducted on a Varian Vista-Pro instrument. Scan electron microscopy (SEM) was conducted via a scanning electron microscope (Hitachi S-4800). High-resolution transmission electron microscopy (HRTEM) and energy-dispersive X-ray (EDX) images were performed on a FEI Tecnai G2 F20 S-TWIN ffield-emissiontransmission electron microscope equipped with an EDX analyzer and operated at 200 kV.

1.3. Electrochemical Measurements

Electrochemical OER measurements were conducted in a standard three-electrode electrochemical cell (Pine Research Instrumentation) with a reversible hydrogen electrode (RHE) configuration controlled by a CHI 760D electrochemistry workstation in O_2-saturated 0.1 M KOH at room temperature. Glassy carbon (GC, 0.196 cm^2), Ag/AgCl, and graphite rod were used as the working, reference, and counter electrodes, respectively. The catalyst ink was prepared by catalyst (10 mg), conductive carbon (Super P Li, 10 mg), Nafion (5 wt%, 100 μL), and absolute ethanol (1 mL). Then, 5 μL of the catalyst ink was transferred onto the surface of the GC substrate and the catalyst loading was about 0.232 mg cm^{-2}. All polarization curves obtained from linear sweep voltammetry (LSV) were recorded at a scan rate of 5 mV s^{-1} from 0.2 to 1.0 V versus Ag/AgCl with a rotation rate of 1600 r.p.m. Electrochemical impedance spectroscopy (EIS) spectra were recorded from 100 kHz to 0.1 Hz at 0.7 V versus Ag/AgCl under an AC voltage of 10 mV. Cyclic voltammetry (CV) tests were used to measure the electrochemical double-layer capacitance (C_{dl}). The potential was swept from 0.2 to 0.3 V versus Ag/AgCl at scan rates of 20, 40, 60, 80, and 100 mV s^{-1}. Chronopotentiometry (CP) was used to measure long-term stabilities under a constant current density of 10 mA cm^{-2}, where the catalysts were deposited onto carbon paper (HCP330 N; hanghai Hesen Electric Co., Ltd) with a loading of approximately 0.5 mg cm^{-2}. The overall water splitting tests were performed in a two-electrode system with catalysts loaded

on Ni foam (mass loading: 3 mg cm^{-2}). Polarization curves were obtained using LSV with a scan rate of 5 mV s^{-1}.

1.4. Assembly of Water Splitting and Zn-air batteries

The overall water splitting tests were performed in a two-electrode system with PSFC and Pt/C (20%, Shanghai Hesen Electric Co., Ltd) loaded on Ni foam (mass loading: 3 mg cm^{-2}) as the anodic and cathodic electrodes, respectively. Polarization curves were obtained using LSV with a scan rate of 5 mV s^{-1}. The home-made Zn-Air battery was assembled with the PSFC loaded on gas diffusion layer electrode, a Zn foil as the metal electrode, and 6 M KOH + 0.2 M $ZnCl_2$ as the electrolyte. For comparison, the Water Splitting and Zn-air batteries were also made from RuO_2 (Aladdin Chemical Reagent Co., Ltd.) and Pt/C.

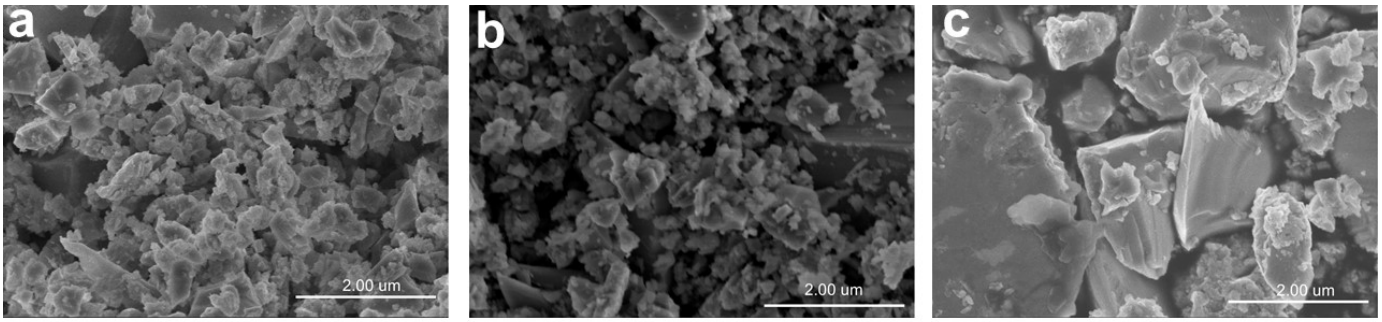

Figure S1. SEM of (a) LSFC, (b) LSFC, and (c) PSFC

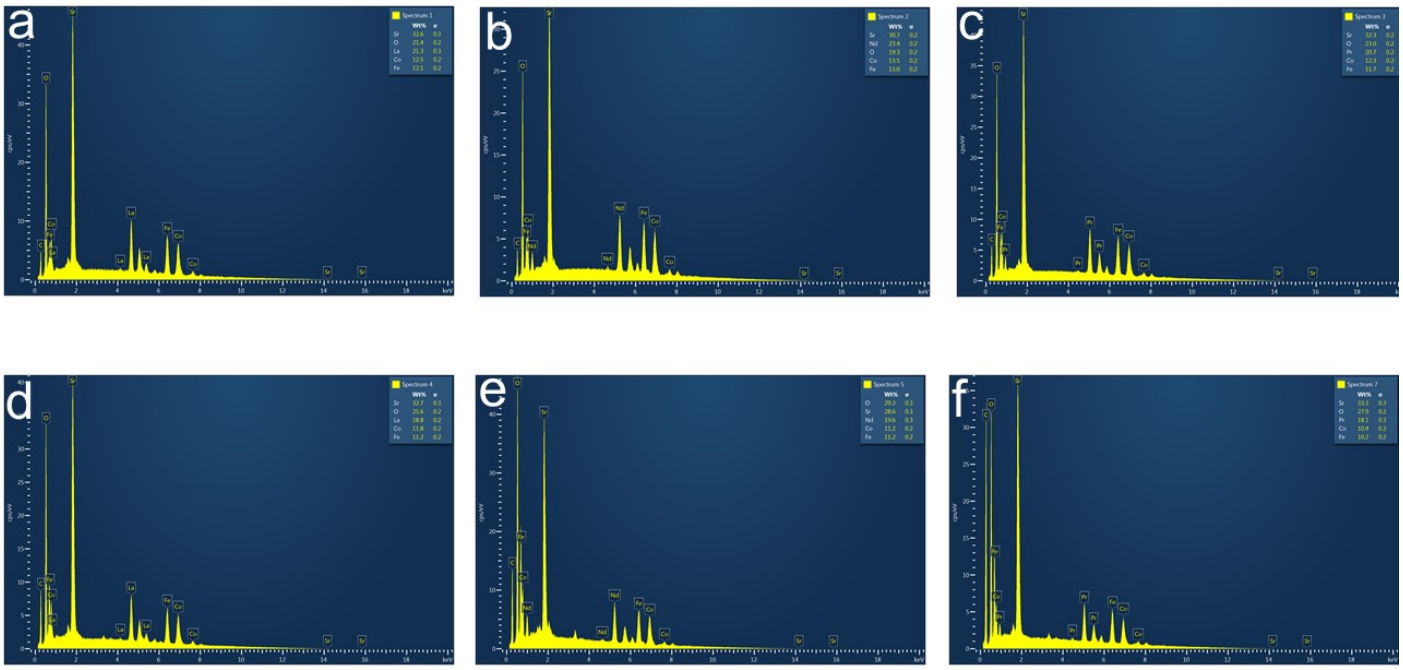

Figure S2. (a-c) EDS of LSFC, NSFC, and PSFC. (d-e) EDS of LSFC, NSFC, and PSFC after

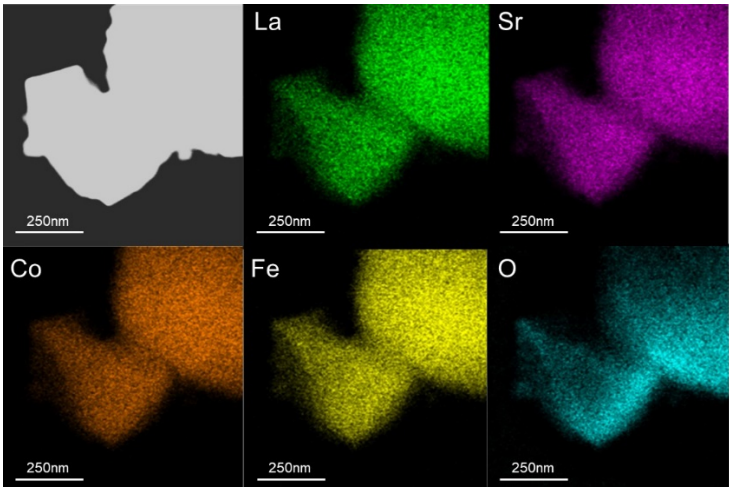

Figure S3. STEM-EDX result of LSCF

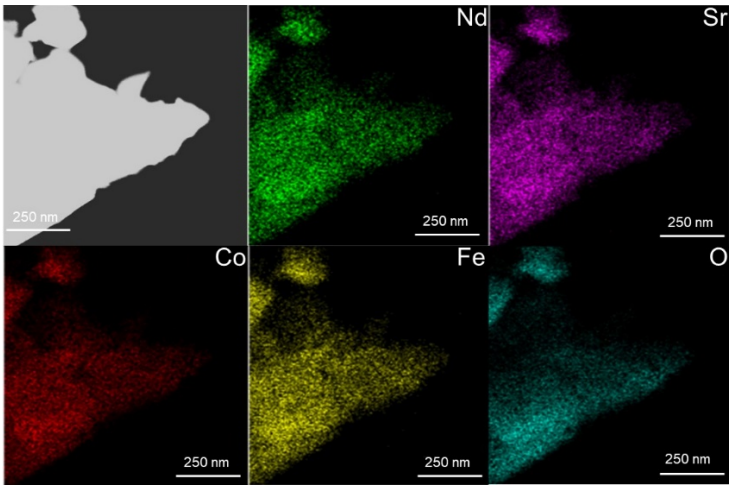

Figure S4. STEM-EDX result of NSCF

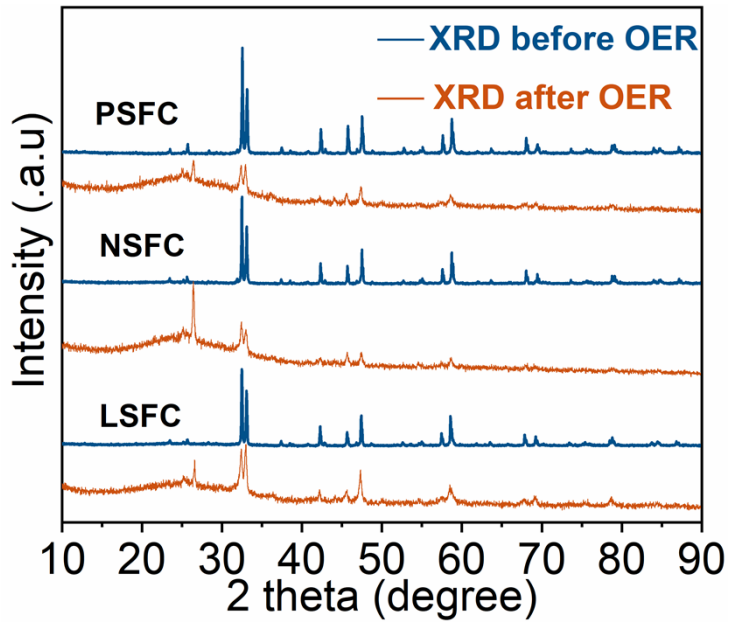

Figure S5. XRD of LSFC, NSFC, and PSFC before and after OER.

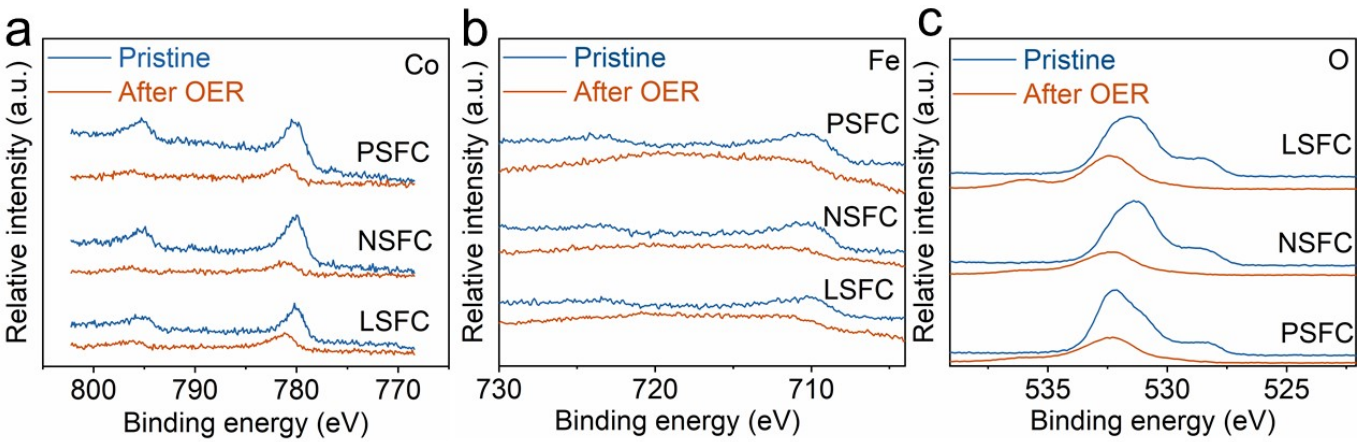

Figure S6. XPS spectrum of LSFC, NSFC, and PSFC before and after OER.

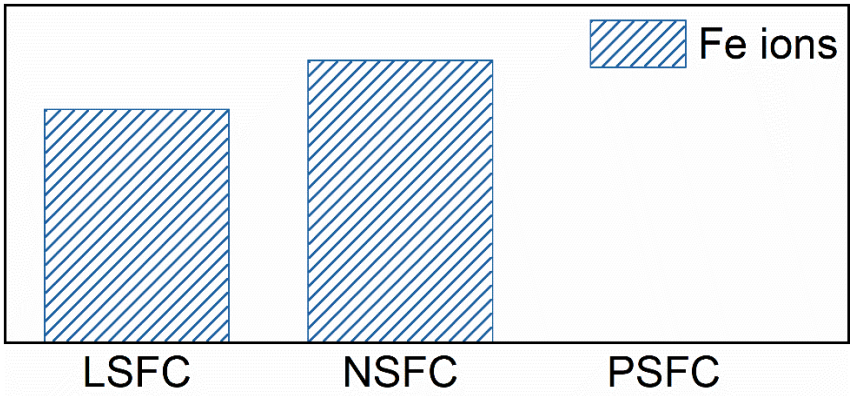

Figure S7. Leaching Fe ions in the electrolyte of LSFC, NSFC, and PSFC after two hours of OER reaction

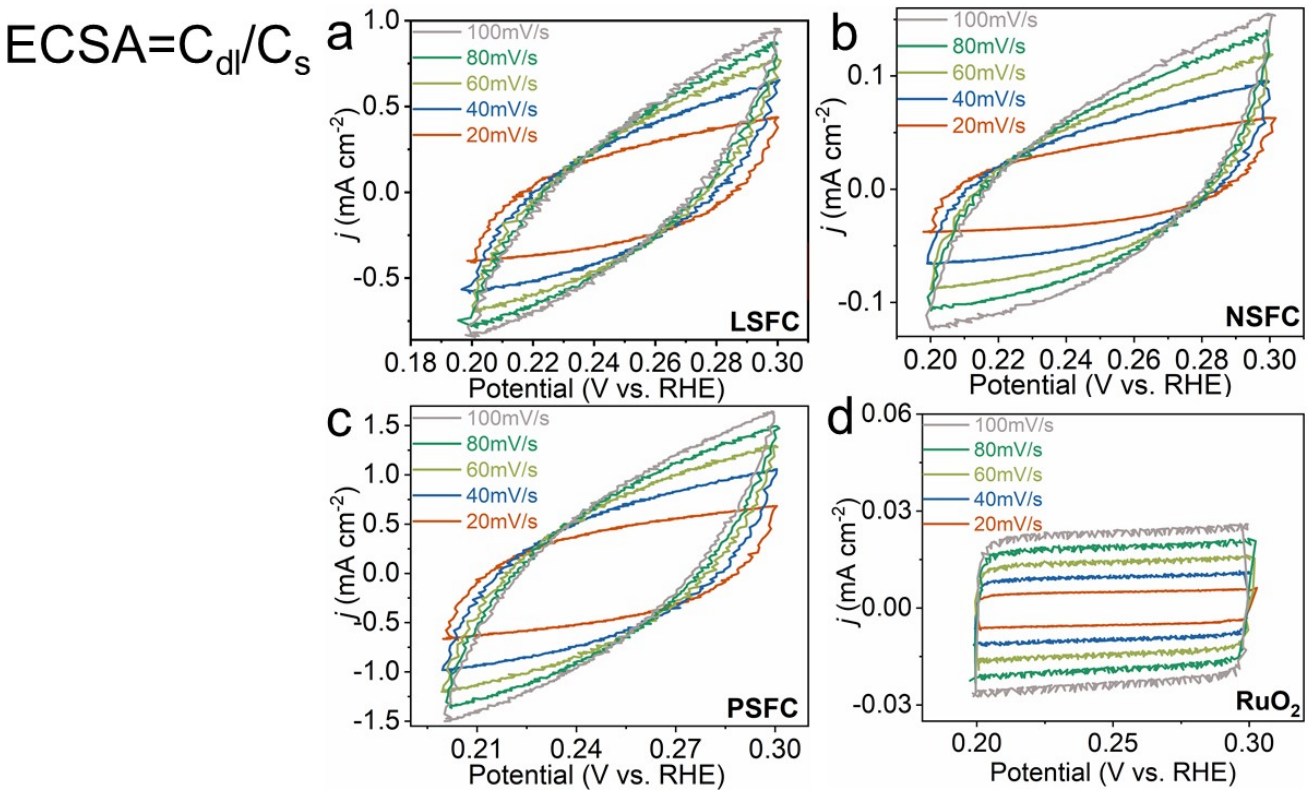

Figure S8. ECSA of (a) LSFC, (b) LSFC, (c) PSFC, and RuO_2

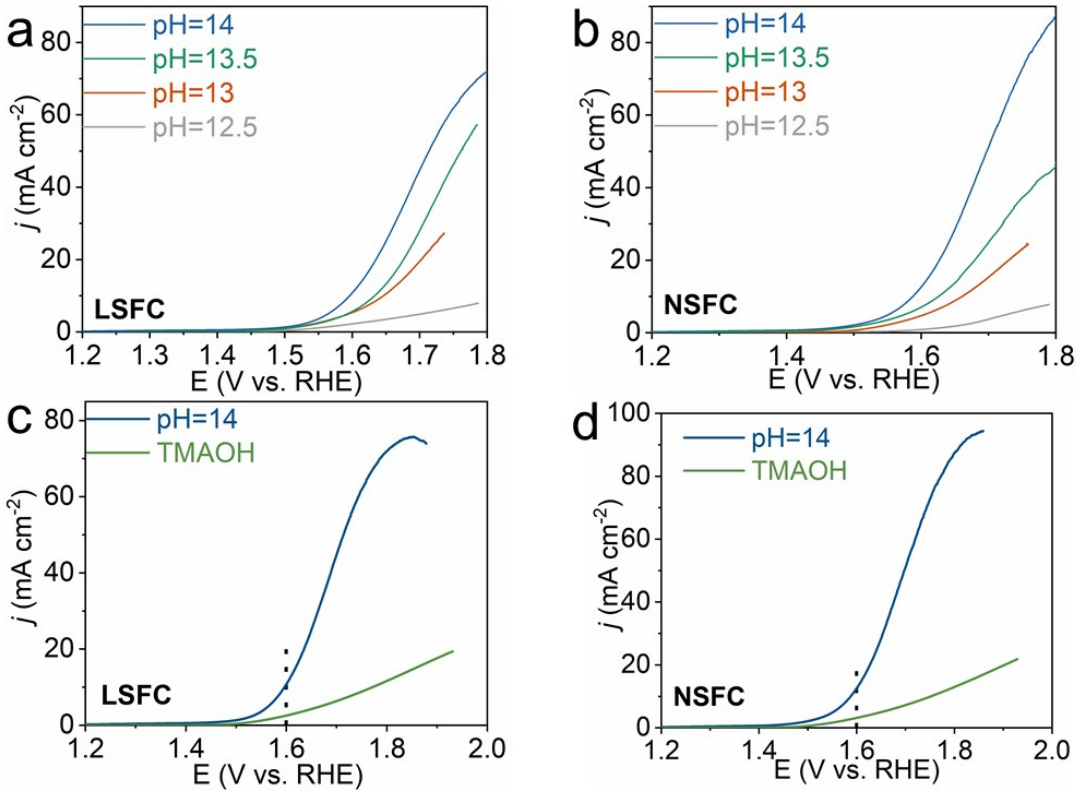

Figure S9. OER polarization curves of (a) LSFC and (b) NSFC under KOH solutions with different pH values. OER polarization curves of (c) LSFC and (d) NSFC under 1M KOH and 1M TMAOH solution.

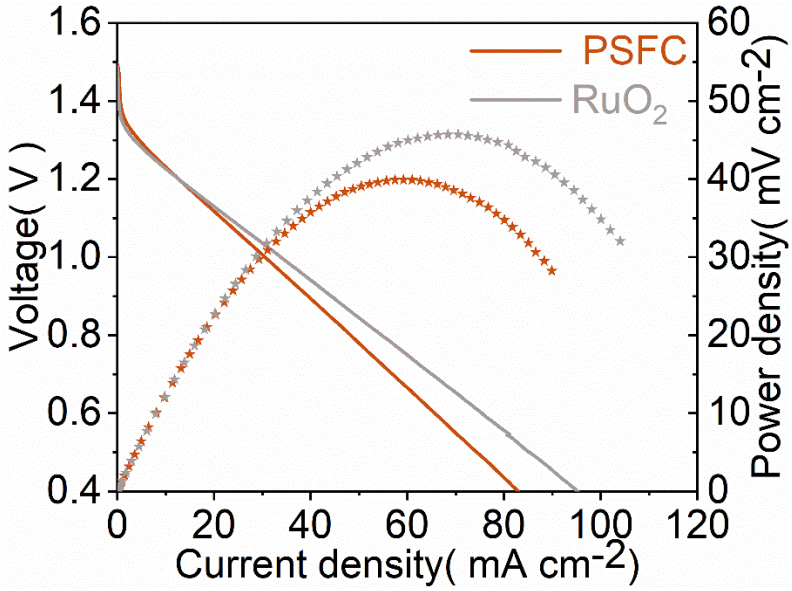

Figure S10. Discharge polarization curves and corresponding power density curves of PSFC and Pt/C+RuO_2 based Zn-air battery.

Table S1. Lattice parameters and structural information of LSFC, NSFC, and PSFC

	LSFC	NSFC	PSFC

Space group	I4/mmm	I4/mmm	I4/mmm
Lattice parameters	a=3.84086	a=3.84086	a=3.84086
	b=3.84086	b=3.84086	b=3.84086
	c=27.86395	c=27.86395	c=27.86395
	α=β=γ=90.0000	α=β=γ=90.0000	α=β=γ=90.0000
Cell volume ($Å^3$)	411.05383	411.05382	411.05382
Density	5.868	5.692	5.938
Co-O bond length (Å)	$C^{o_1-O_2(*18)}$=1.83345	$C^{o_1-O_2(*18)}$=1.82850	$C^{o_1-O_2(*18)}$=1.82856
	$C^{o_1-O_4(*36)}$=1.92043	$C^{o_1-O_4(*36)}$=1.91475	$C^{o_1-O_4(*36)}$=1.91427
	$C^{o_2-O_1(*40)}$=1.92237	$C^{o_2-O_1(*40)}$=1.91669	$C^{o_2-O_1(*40)}$=1.91621
	$C^{o_2-O_2(*10)}$=2.09816	$C^{o_2-O_2(*10)}$=2.09252	$C^{o_2-O_2(*10)}$=2.09256
	$C^{o_2-O_3(*10)}$=1.95884	$C^{o_2-O_3(*10)}$=1.95355	$C^{o_2-O_3(*10)}$=1.95361
Average Co-O length	1.94665	1.941202	1.941042
$R_{wp\%}$	5.24	5.65	5.72
$R_{p\%}$	4.07	4.31	4.47
GOF	1.17	1.24	1.15

Table S2. EDS data of LSFC, NSFC, and PSFC

LSFC	element	La	Sr	Fe	Co
	Atomic ratio (at%)	15.4	39.6	22.5	22.5
NSFC	element	Nd	Sr	Fe	Co
	Atomic ratio (at%)	15.7	37.2	24.2	22.9
PSFC	element	Pr	Sr	Fe	Co

Atomic ratio (at%)	14.9	40.3	22.4	22.4

Table S3. Comparison of OER performance between our catalysts and reported representative active OER electrocatalysts

Catalysts	Electrolyte	Mass loading ($mg.cm^{-2}$)	η_{10}(mV)	Tafel ($mV.dec^{-1}$)	Ref
SFNM@C-6-700	0.1M KOH	0.254	362	48.47	Ref[1]
YCMO	0.1M KOH	0.102	590	73	Ref[2]
LSNMR	0.1M KOH	0.255	430	Not given	Ref[3]
LSF-0.8	0.1M KOH	0.232	370	60.1	Ref[4]
La0.5Sr0.5CoO3-x	0.1M KOH	0.25	400	Not given	Ref[5]
LaMnNiCoO3	0.1M KOH	0.408	370	80.19	Ref[6]
SNCF-BM	0.1M KOH	0.232	420	90	Ref[7]
LCF0.2	0.1M KOH	0.232	340	50	Ref[8]
RP/P-LSCF	0.1M KOH	0.278	324	58	Ref[9]
SCFB-0.3	0.1M KOH	0.232	340	58	Ref[10]
hex-BSCF	0.1M KOH	0.232	340	47	Ref[11]
PBSCF-III	0.1M KOH	0.202	358	52	Ref[12]
NixCo1−xS2	0.1M KOH	0.8	380	Not given	Ref[13]
LaSr3Co1.5Fe1.5O10-δ	0.1M KOH	0.255	388	83.9	Ref[14]
SNCF-NRs	0.1M KOH	0.232	390	61	Ref[15]
Ni-MnO2	0.1M KOH	0.232	420	Not given	Ref[16]
CoNP-PTCOF	0.1M KOH	0.61	450	233	Ref[17]
LSFNF30	0.1M KOH	0.0153	360	44	Ref[18]
SrCoO2.7	0.1M KOH	0.0153	419	67	Ref[18]
NBCFM	0.1M KOH	Not given	359	81	Ref[19]
LBSCOF	0.1M KOH	0.255	470	113	Ref[20]
LNMO-1	0.1M KOH	0.102	370	58	Ref[21]
RP-SCFN	0.1M KOH	0.232	334	57	Ref[22]

La5Ni4O13-δ	0.1M KOH	0.139	420	70	Ref[23]
La5Ni3CoO13-δ	0.1M KOH	0.139	370	35	Ref[23]
RP-PSNC	0.1M KOH	0.2271	450	139	Ref[24]
RP-PSNC/P-PNC	0.1M KOH	0.2271	378	96	Ref[24]
Sr3FeMnO6	0.1M KOH	1.018	590	95	Ref[25]
Sr3TiCoO7-δ	0.1M KOH	Not given	456	120	Ref[26]
Sr2LaMn2O7	0.1M KOH	0.1	589	173	Ref[27]
Ca2LaMn2O7	0.1M KOH	0.1	595	191	Ref[27]
Ca2Sr2Mn2FeO10-δ	0.1M KOH	1.018	510	198	Ref[28]

Table S4. ICP data of the leached ions in electrolytes for the post-OER LSFC, NSFC, and PSFC

		Co mg/L	Fe mg/L
LSFC	After OER	0	0.019
NSFC	After OER	0	0.023
PSFC	After OER	0	0

Table S5. The proportion of Fe^{4+}, Co^{4+}, and oxygen vacancy in LSFC, NSFC, and PSFC.

	LSFC	**NSFC**	**PSFC**
Fe^{4+}/Fe	0.2571	0.4400	0.5671
Co^{4+}/Co	0.1152	0.2920	0.2970
(O_2^{2-}/O^{2-})/O	0.3623	0.4810	0.5419

1. Z. S. Wang, T. Wu, K. Y. Zhu, W. L. Xie, X. F. Zhu and W. S. Yang, Interface modulation of perovskite oxides to simultaneously enhance the activity and stability toward oxygen evolution reaction, *Chemical Engineering Journal*, 2023, **455**.

2. S. C. McGuire, W. Wesley, K. Sasaki, X. Tong and S. S. Wong, Yttrium-based Double Perovskite Nanorods for Electrocatalysis, *Acs Applied Materials & Interfaces*, 2022, DOI: 10.1021/acsami.2c07377.

3. M. Retuerto, F. Calle-Vallejo, L. Pascual, G. Lumbeeck, M. T. Fernandez-Diaz, M. Croft, J. Gopalakrishnan, M. A. Pena, J. Hadermann, M. Greenblatt and S. Rojas, La1.5Sr0.5NiMn0.5Ru0.5O6 Double Perovskite with Enhanced ORR/OER Bifunctional Catalytic Activity, *Acs Applied Materials & Interfaces*, 2019, **11**, 21454-21464.

4. S. X. She, J. Yu, W. Q. Tang, Y. L. Zhu, Y. B. Chen, J. Sunarso, W. Zhou and Z. P. Shao, Systematic Study of Oxygen Evolution Activity and Stability on La1-xSrxFeO3-delta Perovskite Electrocatalysts in Alkaline Media, *Acs Applied Materials & Interfaces*, 2018, **10**, 11715-11721.

5. G. X. Liu, H. B. Chen, L. Xia, S. Q. Wang, L. X. Ding, D. D. Li, K. Xiao, S. Dai and H. H. Wang, Hierarchical Mesoporous/Macroporous Perovskite La0.5Sr0.5CoO3-x Nanotubes: A Bifunctional Catalyst with Enhanced Activity and Cycle Stability for Rechargeable Lithium Oxygen Batteries, *Acs Applied Materials & Interfaces*, 2015, **7**, 22478-22486.

6. J. Sun, L. Du, B. Y. Sun, G. K. Han, Y. L. Ma, J. J. Wang, H. Huo, P. J. Zuo, C. Y. Du and G. P. Yin, A bifunctional perovskite oxide catalyst: The triggered oxygen reduction/evolution electrocatalysis by moderated Mn-Ni co-doping, *Journal of Energy Chemistry*, 2021, **54**, 217-224.

7. Y. Zhu, W. Zhou, Z.-G. Chen, Y. Chen, C. Su, M. O. Tade and Z. Shao, SrNb0.1Co0.7Fe0.2O3-delta Perovskite as a Next-Generation Electrocatalyst for Oxygen Evolution in Alkaline Solution, *Angewandte Chemie-International Edition*, 2015, **54**, 3897-3901.

8. Y. Zhu, W. Zhou, Y. Chen, J. Yu, M. Liu and Z. Shao, A High-Performance Electrocatalyst for Oxygen Evolution Reaction: LiCo0.8Fe0.2O2, *Advanced Materials*, 2015, **27**, 7150-+.

9. Y. L. Zhu, Q. Lin, Z. W. Hu, Y. B. Chen, Y. C. Yin, H. A. Tahini, H. J. Lin, C. T. Chen, X. W. Zhang, Z. P. Shao and H. T. Wang, Self-Assembled Ruddlesden-Popper/Perovskite Hybrid with Lattice-Oxygen Activation as a Superior Oxygen Evolution Electrocatalyst, *Small*, 2020, **16**.

10. S. X. She, Y. L. Zhu, Y. B. Chen, Q. Lu, W. Zhou and Z. P. Shao, Realizing Ultrafast Oxygen Evolution by Introducing Proton Acceptor into Perovskites, *Advanced Energy Materials*, 2019, **9**.

11. Y. L. Zhu, H. A. Tahini, Z. W. Hu, Z. G. Chen, W. Zhou, A. C. Komarek, Q. Lin, H. J. Lin, C. T. Chen, Y. J. Zhong, M. T. Fernandez-Diaz, S. C. Smith, H. T. Wang, M. L. Liu and Z. P. Shao, Boosting Oxygen Evolution Reaction by Creating Both Metal Ion and Lattice-Oxygen Active Sites in a Complex Oxide, *Advanced Materials*, 2020, **32**.

12. B. Zhao, L. Zhang, D. Zhen, S. Yoo, Y. Ding, D. Chen, Y. Chen, Q. Zhang, B. Doyle, X. Xiong and M. Liu, A tailored double perovskite nanofiber catalyst enables ultrafast oxygen evolution, *Nature Communications*, 2017, **8**.

13. Y. J. Zhong, X. M. Xu, P. Y. Liu, R. Ran, S. P. Jiang, H. W. Wu and Z. P. Shao, A Function-Separated Design of Electrode for Realizing High-Performance Hybrid Zinc Battery, *Advanced Energy Materials*, DOI: 10.1002/aenm.202002992.

14. S. Liu, H. Luo, Y. Li, Q. Liu and J.-L. Luo, Structure-engineered electrocatalyst enables highly active and stable oxygen evolution reaction over layered perovskite LaSr3Co1.5Fe1.5O10-delta, *Nano Energy*, 2017, **40**, 115-121.

15. Y. L. Zhu, W. Zhou, Y. J. Zhong, Y. F. Bu, X. Y. Chen, Q. Zhong, M. L. Liu and Z. P. Shao, A Perovskite Nanorod as Bifunctional Electrocatalyst for Overall Water Splitting, *Advanced Energy Materials*, 2017, **7**.

16. Y. J. Zhong, J. Dai, X. M. Xu, C. Su and Z. P. Shao, Facilitating Oxygen Redox on Manganese Oxide Nanosheets by Tuning Active Species and Oxygen Defects for Zinc-Air Batteries, *Chemelectrochem*, 2020, **7**, 4949-4955.

17. J. H. Park, C. H. Lee, J.-M. Ju, J.-H. Lee, J. Seol, S. U. Lee and J.-H. Kim, Bifunctional Covalent Organic Framework-Derived Electrocatalysts with Modulated p-Band Centers for Rechargeable Zn-Air Batteries, *Advanced Functional Materials*, 2021, **31**.

18. R. P. Forslund, W. G. Hardin, X. Rong, A. M. Abakumov, D. Filimonov, C. T. Alexander, J. T. Mefford, H. Iyer, A. M. Kolpak, K. P. Johnston and K. J. Stevenson, Exceptional electrocatalytic oxygen evolution via tunable charge transfer interactions in La0.5Sr1.5Ni1-xFexO4 +/-delta Ruddlesden-Popper oxides, *Nature Communications*, 2018, **9**.

19. N.-I. Kim, Y. J. Sa, T. S. Yoo, S. R. Choi, R. A. Afzal, T. Choi, Y.-S. Seo, K.-S. Lee, J. Y. Hwang, W. S. Choi, S. H. Joo and J.-Y. Park, Oxygen-deficient triple perovskites as highly active and durable bifunctional electrocatalysts for oxygen electrode reactions, *Science Advances*, 2018, **4**.

20. B. Hua, M. Li, W. Y. Pang, W. Q. Tang, S. L. Zhao, Z. H. Jin, Y. M. Zeng, B. S. Amirkhiz and J. L. Luo, Activating p-Blocking Centers in Perovskite for Efficient Water Splitting, *Chem*, 2018, **4**, 2902-2916.

21. Y. Tong, J. C. Wu, P. Z. Chen, H. F. Liu, W. S. Chu, C. Z. Wu and Y. Xie, Vibronic Superexchange in Double Perovskite Electrocatalyst for Efficient Electrocatalytic Oxygen Evolution, *Journal of the American Chemical Society*, 2018, **140**, 11165-11169.

22. Y. Zhu, H. A. Tahini, Z. Hu, Y. Yin, Q. Lin, H. Sun, Y. Zhong, Y. Chen, F. Zhang, H.-J. Lin, C.-T. Chen, W. Zhou, X. Zhang, S. C. Smith, Z. Shao and H. Wang, Boosting oxygen evolution reaction by activation of lattice-oxygen sites in layered Ruddlesden-Popper oxide, *Ecomat*, 2020, **2**, e12021.

23. S. R. Choi, J.-I. Lee, H. Park, S. W. Lee, D. Y. Kim, W. Y. An, J. H. Kim, J. Kim, H.-S. Cho and J.-Y. Park, Multiple perovskite layered lanthanum nickelate Ruddlesden-Popper systems as highly active bifunctional oxygen catalysts, *Chem. Eng. J.*, 2021, **409**,128226.

24. G. Pan, Y. Deng, L. Zhao, H. Wang, R. Wang, J. Jin, Y. Gong and B. He, In-situ construction of Ruddlesden-Popper/perovskite heterointerface induces efficient bifunctional oxygen electrocatalyst for rechargeable zinc-air batteries, *Electrochim. Acta*, 2022, **424**, 140673.

25. S. B. Karki, R. K. Hona and F. Ramezanipour, $Sr_3Mn_2O_6$ and Sr_3FeMnO_6 for oxygen and hydrogen evolution electrocatalysis, *J. Solid State Electrochem.*, 2022, **26**, 1303-1311.

26. C. C. W. Kananke-Gamage and F. Ramezanipour, Isostructural Oxides $Sr_3Ti_{2-x}M_xO_{7-delta}$ (M = Mn, Fe, Co; x=0, 1) as Electrocatalysts for Water Splitting, *Inorganics*, 2023, **11**, 172.

27. C. C. W. Kananke-Gamage and F. Ramezanipour, Effect of structural symmetry on magnetic, electrical and electrocatalytic properties of isoelectronic oxides $A_2LaMn_2O_7$ (A= Sr^{2+}, Ca^{2+}), *J. Phys. Chem. Solids*, 2022, **171**, 111013.

28. S. B. Karki, R. K. Hona and F. Ramezanipour, Electrocatalytic activity and structural transformation of $Ca_2Sr_2Mn_2MO_{10-delta}$ (M = Fe, Co), *Ionics*, 2022, **28**, 397-406.